Simulation and Optimization of Colloidal Micro-Pumps

D. Liu*, M. Maxey** and G. Karniadakis

* Division of Applied Mathematics, Brown University
Providence, RI 02912, USA, dong@dam.brown.edu
** maxey@dam.brown.edu

ABSTRACT

A fast algorithm for particulate microflows[1] has been used to simulate the 3D micro-colloidal pumps tested in the experiments conducted by Terray et at.[2]. The Force-Coupling Method and a penalty method were implemented in a spectral element code to simulate the dynamics of both peristaltic and gear pumps. Parametric studies were made for different viscosity, channel width and frequency to better understand the inherent mechanisms.

Keywords: Force-coupling method, Micro-flow devices, Spectral elements

1 INTRODUCTION

The manipulation of colloidal particles by magnetic forces or by optical trapping in a microchannel opens the possibility of devising new strategies for pumping or mixing in microflows. Terray et al. [2] have demonstrated experimentally the operation of microdevices in which colloidal particles, 1-3 μm in diameter, are manipulated in an optical trap to control the flow in microchannels. Numerical simulations provide a means to test the performance of such devices and provide additional data unavailable from experiments. We present in this paper a short summary of the Force-Coupling Method(FCM) that had been developed by Maxey & Patel [3] and Lomholt et al. [4] for the efficient simulation of particulate dynamics in liquid flows. The method is based on representing the particles by force multipoles distributed over a finite volume. This approach has been tested against full DNS by Liu et al. [1] and shown to be an accurate and efficient way to simulate particulate microflows. We validate the method by a pressure-driven flow and provide two examples of pumping flows.

2 SIMULATION METHOD

The equations of fluid motion for the fluid velocity $\mathbf{u}(\mathbf{x},t)$ are

$$\rho\frac{D\mathbf{u}}{Dt} = -\nabla p + \mu\nabla^2\mathbf{u} + \mathbf{f}(\mathbf{x},t) \qquad (1)$$

$$\nabla\cdot\mathbf{u} = 0 \qquad (2)$$

where ρ, p and μ are the fluid density, pressure and viscosity respectively. The source term $\mathbf{f}(\mathbf{x},t)$ represents the sum of two-way coupling forces from each spherical particle n centered at $\mathbf{Y}^{(n)}(t)$. For a single particle,

$$f_i(\mathbf{x},t) = F_i\Delta(\sigma_1,\mathbf{x}-\mathbf{Y}(t)) + G_{ij}\frac{\partial\Delta(\sigma_2,\mathbf{x}-\mathbf{Y}(t))}{\partial x_j} \qquad (3)$$

where both $\Delta(\sigma_1,\mathbf{x})$ and $\Delta(\sigma_2,\mathbf{x})$ are Gaussian distribution functions of the same form as

$$\Delta(\sigma_1,\mathbf{x}) = (2\pi\sigma_1^2)^{-3/2}\exp(-\mathbf{x}^2/(2\sigma_1^2)) \qquad (4)$$

The first term in (3) is a finite force monopole of strength $\mathbf{F}$ while the second term is a force dipole of strength G_{ij}. The monopole strength is set by the sum of the external forces, such as magnetic force or gravity force, acting on the particle as well as the inertia of the particle.

The values of the length scales σ_1 and σ_2 in (4) are directly related to the particle radius with $a/\sigma_1 = \sqrt{\pi}$ and $a/\sigma_2 = (6\sqrt{\pi})^{1/3}$ as given by Maxey & Patel [3], Lomholt et al. [4], and Lomholt [5].

The symmetric, stresslet component of the force dipole G_{ij} is set through a dipole iteration scheme to minimize the integral-averaged strain rate inside the volume nominally occupied by particles, down to 1% of the ratio of the particle velocity to its radius, see Liu et al. [1]. The antisymmetric components correspond to torques acting on the particle.

The velocity of each particle $\mathbf{V}(t)$ is evaluated from a volume integral of the local fluid velocity as

$$\mathbf{V}(t) = \int_D \mathbf{u}(\mathbf{x},t)\Delta(\sigma_1,\mathbf{x}-\mathbf{Y}(t))\,d^3\mathbf{x} \qquad (5)$$

The angular velocity $\mathbf{\Omega}$ of the particle is computed by a local volume average of the fluid vorticity $\mathbf{W}$(x,t)

$$\mathbf{\Omega} = \frac{1}{2}\int_D \mathbf{W}(\mathbf{x},t)\Delta(\sigma_2,\mathbf{x}-\mathbf{Y}(t))\,d^3\mathbf{x} \qquad (6)$$

The new position of each particle is calculated as

$$\mathbf{V}(t) = \frac{d\mathbf{Y}(t)}{dt} \qquad (7)$$

A spectral/hp element method has been used to solve for the primitive variables $\mathbf{u}, p$ in the Navier-Stokes equations. Further details are given by Karniadakis & Sherwin [6].

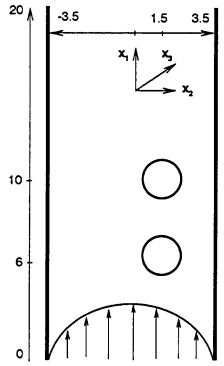

Figure 1: Sketch of flow configuration of two particles in a pressure-driven flow.

3 PRESSURE-DRIVEN FLOW

We validate the simulation method with a pressure-driven flow with channel Reynolds number about 6. The dimensions of the channel scaled by the particle radius $a = 1$ are $0 < x_1 < 20$ streamwise, and $-3.5 < x_2, x_3 < 3.5$ for both x_2 and x_3 directions. Two particles are placed in the channel with coordinates as $Y_1 = 10$, $Y_2 = 1.5$, $Y_3 = 0$ for the first particle and $Y_1 = 6$, $Y_2 = 1.5$, $Y_3 = 0$ for the second as shown in figure 1. Periodic boundary conditions were applied in both x_1 and x_3 directions while no-slip boundary conditions were specified on each rigid channel wall at $x_2 = \pm 3.5$. A constant, streamwise pressure gradient of dimensionless value 0.2 was imposed to drive the flow. In the FCM simulation, a mesh of 480 non-uniform hexahedral elements was finally adopted, with a sixth order modified Jacobi polynomial expansion for each element.

In order to fix the particles in their position, restoring forces (8) were computed via a penalty method and included in the force monopole term. To hold the particles from rotating, restoring torques (9) were computed similarly and added in the anti-symmetric part of the force dipole term. λ_1 has the dimension $\mu\nu/a$ and λ_2 has $\mu\nu a$. The constants c_1 and c_2 control the speed of convergence and do not affect the final results.

$$\frac{d\mathbf{F}^{Restore}(t)}{dt} = c_1\lambda_1\mathbf{V}(t) \tag{8}$$

$$\frac{dG_{ij}}{dt} = c_2\lambda_2\epsilon_{ijk}\Omega_k \tag{9}$$

In the DNS simulation, the final results were given with 9th-order polynomial expansion on a structured mesh of 768 hexahedral elements in the volume outside particles and inside channel boundaries. Similar boundary conditions as in the FCM were imposed. In addition, on particles' surface, rigid no-slip boundary conditions were imposed.

	Force in x_2	*Force in* x_1	*Torque in* x_2
FCM Par. 1	-0.50	-21.31	-3.08
DNS Par. 1	0.52	20.43	3.18
FCM Par. 2	1.66	-22.22	-3.19
DNS Par. 2	-1.63	21.41	3.29

Table 1: Comparison of forces and torques on each particle from both FCM and DNS simulation.

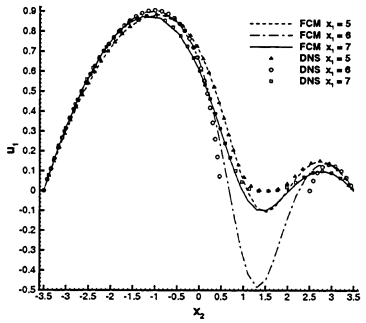

Figure 2: Streamwise fluid velocity u_1 profiles versus x_2.

From both the well converged DNS and FCM results, the lift, drag and torque on each particle in DNS are given in dimensionless units in table 1. The corresponding values in the table for FCM are *restoring* forces and torques. Since they act on each particle to prevent it from translating and rotating, the signs are just the opposite of the DNS data.

In figure 2, the streamwise fluid velocity u_1 profiles versus x_2 are plotted from the plane $x_3 = 0$ at different x_1 locations as denoted in the legend for both FCM and DNS results. Figure 3 shows the streamwise fluid velocity u_1 versus x_1 from the plane $x_3 = 0$ with x_2=1.5 for both FCM and DNS results. In the FCM formulation the boundary conditions on the particle surface are not imposed explicitly but only included implicitly in (5). As a result, the FCM and DNS results differ around the

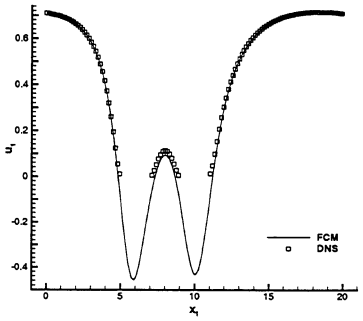

Figure 3: Streamwise fluid velocity u_1 profiles along x_1.

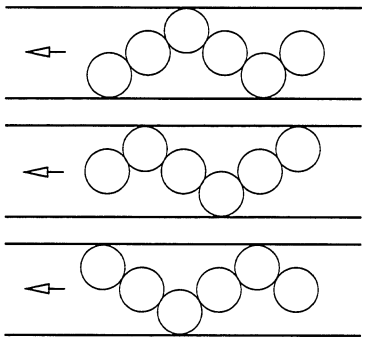

Figure 4: Micro-peristaltic pump showing particle positions at t=0,1,2 for case II in table 2.

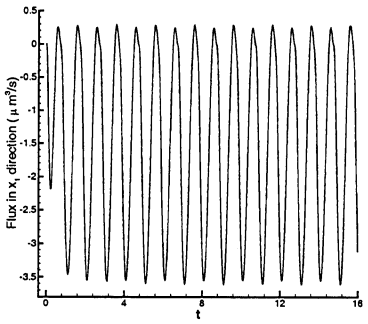

Figure 5: Evolution of volume flux Q(t) for case V in table 2.

particle surface although good agreement is achieved in general.

4 FCM SIMULATION OF PERISTALTIC PUMP

Terray et al. [2] reported that by manipulating colloidal microspheres within a microchannel, a peristaltic pump could be created. We simulate the peristaltic pump accordingly with 6 particles of diameter 3 microns in a microchannel of dimension 24 microns in x_1, 6 microns in x_2, and 4 microns in x_3. Periodic boundary conditions were applied at the channel ends at $x_1 = 0$ and 24 microns while no-slip boundary conditions were specified on the four rigid side-walls of the channel in the x_2 and x_3 directions.

A transverse traveling wave motion of the following form was needed for each particle to produce a pumping effect:

$$Y_2 = Asin[\omega t + (i-1)\frac{\pi}{2}] \qquad (10)$$

where $A = 1.5$ microns, is the amplitude; ω is the pump frequency controlling parameter; i=0 to 5 is the particle numbering index. To achieve this traveling wave motion, a set of forces $\mathbf{F}$ in the x_2 direction (perpendicular to streamwise x_1 direction) was applied to each particle:

$$F_2 = -Psin[\omega t + (i-1)\frac{\pi}{2}] \qquad (11)$$

where the magnitude of P was scaled for different ω to produce the motion (10). In addition, inter-particle forces are also included in the force monopole term to maintain contact between adjacent particles without overlapping. When a particle touches a wall, a contact force is automatically activated to prevent it from entering the wall. By varying ω and the kinematic viscosity ν we achieved different pump periods T and average volume fluxes Q over a range of operating conditions. Peak Reynolds number ranges from 30 to 6×10^{-4}. A summary of the parameters and results, such as time-averaged volume flux Q scaled by $a^3\omega$ and the nondimensional frequency $\omega a^2/\nu$, for different cases is shown in table 2.

Case	I	II	III	IV	V
ω	4π	$\pi/2$	$\pi/12$	$\pi/12$	$\pi/2$
T	0.5	4	24	24	4
$\omega a^2/\nu$	28.3	3.5	0.6	$5.9\text{x}10^{-4}$	$3.5\text{x}10^{-3}$
$Q/a^3\omega$	0.38	0.4	0.44	0.37	0.31

Table 2: A summary of the parameters and results for different cases.

Figure 4 shows the traveling wave motion towards the left at three moments for case II. The arrows denote the direction of bulk fluid motion. Figure 5 shows the evolution of volume flux. Because of the wave motion, the volume flux also has a harmonic response after initial transients. The overall negative values of $Q(t)$ show that the net flow is in the direction of the traveling wave. A sequence of velocity vectors is presented in figure 6. Increasing the spanwise width of the channel leads to an increase in the net volume flux. This is shown in figure 7. Increasing the width beyond 15 microns has little effect; the volume flux grows asymptotically to a maximum value.

5 FCM SIMULATION OF GEAR PUMP

We simulate a gear pump similarly - the flow generated by two counter-rotating pairs of particles in a lobed channel, as illustrated in figure 8. This configuration was also shown in experiments by Terray et al. [2] to produce a net flow. The geometry of the microchannel is 19 microns in x_1, 6 microns in x_2, and 4 microns in x_3. In the middle of the channel is a cylindric cavity with radius 3.5 microns. Two pairs of particles with diameter 3 microns counter-rotate with a 90 degree phase

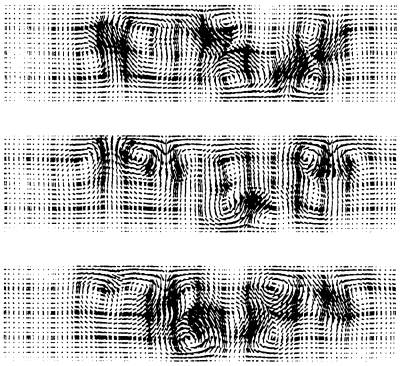

Figure 6: Velocity vectors field at t=2,3,4 in a peristaltic pump for case II.

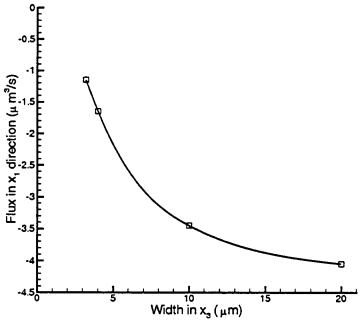

Figure 7: The effect of channel width on volume flux in peristaltic pump for case V.

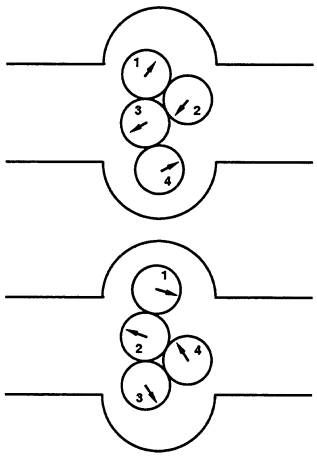

Figure 8: Gear pump configuration with two counter-rotating pairs of particles in a lobed microchannel.

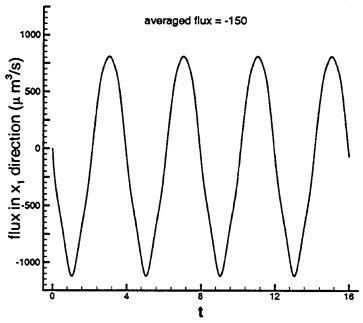

Figure 9: Evolution of gear pump with a period T=4.

angle offset. Periodic boundary conditions were applied at the channel ends at $x_1 = 0$ and 19 microns while no-slip boundary conditions were specified on the four rigid side-walls in the x_2 and x_3 directions. To produce the counter-rotating motion of the particles, periodic forces were applied to each particle and added into the force monopole term of $\mathbf{f}(\mathbf{x}, t)$ in (1). The particle velocity was computed from (7) and verified to match the prescribed motion. In this way the coupled motion of both particulate and fluid phase was realized numerically. Figure 9 shows the fluctuations of the volume flux. Although it has a back and forth motion, the overall effect is to produce a net displacement of fluid from one side to the other.

REFERENCES

[1] D. Liu, M.R. Maxey & G.E. Karniadakis, Journal of Microelectromechanical Systems, Vol. 11, No. 6, 691-702, 2002.

[2] A. Terray, J. Oakley & D.W. Marr, Science Vol. 296, 1841-1844, 2002.

[3] M.R. Maxey & B.K. Patel, Int. J. Multiphase Flow 9, 1603-1626, 2001.

[4] S. Lomholt, B. Stenum & M.R. Maxey, Int. J. Multiphase Flow 28, 225-246, 2002.

[5] S. Lomholt, Numerical Investigations of Macroscopic Particle Dynamics in Microflows, Ph.D. dissertation, Risoe, National Laboratory, Roskilde, Denmark.

[6] G.E. Karniadakis & S. J. Sherwin, Spectral/hp Element Methods for CFD, Oxford University Press, 1999.